Low-temperature magnetic order and spin dynamics in $YbRh_2Si_2$

K. Ishida,[1,2,*] D. E. MacLaughlin,[1] Ben-Li Young,[1] K. Okamoto,[2] Y. Kawasaki,[2,†] Y. Kitaoka,[2] G. J. Nieuwenhuys,[3] R. H. Heffner,[4] O. O. Bernal,[5] W. Higemoto,[6] A. Koda,[6] R. Kadono,[6] O. Trovarelli,[7] C. Geibel,[7] and F. Steglich[7]

[1]*Department of Physics, University of California, Riverside, California 92521-0413, USA*

[2]*Department of Physical Science, Graduate School of Engineering Science, Osaka University, Toyonaka, Osaka 560-8531, Japan*

[3]*Kamerlingh Onnes Laboratory, Leiden University, 2500 RA Leiden, The Netherlands*

[4]*MS K764, Los Alamos National Laboratory, Los Alamos, New Mexico 87545, USA*

[5]*Department of Physics and Astronomy, California State University, Los Angeles, California 90032, USA*

[6]*Meson Science laboratory, Institute of Materials Structure Science, High Energy Accelerator Research Organization (KEK), 1-1 Oho, Tsukuba, Ibaraki 305-0801, Japan*

[7]*Max-Planck Institute for Chemical Physics of Solids, D-01187 Dresden, Germany*

(Received 19 March 2003; published 3 November 2003)

Muon spin rotation and relaxation experiments have been carried out in single crystals of $YbRh_2Si_2$, a compound that exhibits non-Fermi-liquid (NFL) behavior associated with a quantum critical point (QCP) at $T=0$. The zero-field muon relaxation rate is found to be independent of temperature down to 100 mK but to increase below $\sim$70 mK, which suggests magnetic order at low temperatures. From the relation between the internal field at the μ^+ stopping site and the hyperfine coupling constant the ordered Yb^{3+} moment is very small, $\sim 2\times 10^{-3}\mu_B$. Muon spin rotation linewidths in a transverse field of 6 kOe indicate a homogeneous susceptibility down to 2 K, which is an order of magnitude lower than the characteristic (Kondo) temperature $T_K \approx 25$ K. This is evidence against the importance of disorder-driven NFL mechanisms in $YbRh_2Si_2$. In longitudinal magnetic fields the muon spin-lattice relaxation function $G(t)$ is exponential, again indicative of a homogeneous system. The relaxation obeys the time-field scaling relation $G(t,H)=G(t/H)$, which suggests long-lived spin correlations at low temperatures. The Yb^{3+} spin dynamics derived from muon spin relaxation appear to be intimately related to critical magnetic fluctuations near the QCP.

DOI: 10.1103/PhysRevB.68.184401 PACS number(s): 75.40.−s, 76.75.+i, 75.20.Hr

I. INTRODUCTION

Non-Fermi-liquid (NFL) behavior and quantum critical (QC) phenomena in strongly correlated electron systems are among the most intensively studied subjects in condensed matter physics.[1] NFL behavior is observed in a number of *f*-electron systems, which show pronounced deviations from conventional Landau Fermi-liquid properties when they are tuned through a quantum critical point (QCP) by varying a control parameter such as doping, pressure, or magnetic field.[2] The character of magnetic fluctuations near a QCP has been investigated not only to elucidate the behavior of magnetic order in metals but also with relation to unconventional superconductivity, since superconductivity with Cooper pairs having finite angular momentum sometimes appears after suppression of the magnetic order by applied pressure.[3–5] QC magnetic fluctuations have been proposed as a promising pairing mechanism for this unconventional superconductivity, the character of which has not been fully understood.

When a compound is close to its QCP, due to the development of spin fluctuations that mediate interactions between quasiparticles, quasiparticle masses, and scattering cross sections show pronounced temperature dependence.[2] These effects are one mechanism for NFL behavior such as anomalous temperature dependence of the deviation $\Delta\rho=\rho(T)-\rho_0$ of the electrical resistivity from its zero-temperature value ($\Delta\rho\propto T^{\alpha}$, $1\leqslant\alpha<2$), and the *f*-electron specific heat coefficient ($\Delta C/T\propto -\ln T$).[1,2,6] This contrasts with the Fermi-liquid behavior seen in ordinary metals ($\Delta\rho\propto T^2$ and $\Delta C/T=$const). NFL behavior has been observed in alloy systems such as $CeCu_{6-x}R_x(R=\mathrm{Au,Ag})$ (Ref. 7) and $UCu_{5-x}Pd_x$,[8] and in antiferromagnetic (AFM) heavy-fermion (HF) compounds such as $CeIn_3$ (Ref. 4) and $CePd_2Si_2$ (Ref. 9) in which the magnetic order is suppressed by applying pressure.

Microscopic techniques such as nuclear magnetic resonance (NMR), nuclear quadrupole resonance (NQR), and muon spin rotation and relaxation (μSR) are powerful tools with which to investigate QC magnetic fluctuations. While NQR[10–12] and other experiments have revealed pressure-induced superconductivity, few NMR and μSR experiments under pressure have been reported to date due to experimental difficulties. In particular μSR studies of NFL behavior have been limited to alloy systems at ambient pressure. NMR and μSR experiments on the NFL alloys $UCu_{5-x}Pd_x$, $x=1.0$ and 1.5, have revealed strongly inhomogeneous spin fluctuations and the time-field scaling expected from glassy dynamics; the μSR results suggest a quantum spin-glass state near the QCP.[13] But disorder may strongly influence the spin fluctuation behavior, so that it is quite important to investigate whether or not inhomogeneous behavior is seen even in nominally ordered stoichiometric compounds near the QCP. This might give important information about QC magnetic fluctuations and μSR experiments on structurally ordered compounds in which NFL behavior can be observed at ambient pressure would be highly desirable.

The NFL compound $YbRh_2Si_2$ appears to be a suitable system for the study of such ''clean'' NFL physics. $YbRh_2Si_2$ crystallizes in the $ThCr_2Si_2$ structure, and appears to be lo-

cated in the vicinity of a QCP from a number of bulk measurements.[14,15] The resistivity and specific heat at low temperatures show $\Delta\rho \propto T$ and $\Delta C/T \propto -\ln T$ over a temperature range of more than a decade. Recent ^{29}Si NMR studies[16] revealed that at 1.5 kOe the nuclear spin-lattice relaxation rate divided by temperature $1/T_1T$ continues to increase down to 50 mK, indicative of growing magnetic correlation even at the lowest temperature. The NFL behavior is suppressed by the application of an external magnetic field, and Fermi-liquid behavior is recovered. In addition, anomalies at 70 mK in the resistivity, ac susceptibility, and specific heat have been associated with an AFM transition at that temperature.[15,17,18] A small magnetic field of $\sim$500 Oe in the *ab* plane is enough to suppress this transition. These results indicate that $YbRh_2Si_2$ undergoes a magnetic phase transition for very low temperatures and magnetic fields, but is quite close to an AFM QCP.

In order to investigate the 70-mK anomaly and the character of spin fluctuations at zero and weak magnetic fields, we have carried out zero-field (ZF) and longitudinal-field (LF) (i.e., muon spin polarization parallel to the applied field) muon spin relaxation experiments on $YbRh_2Si_2$. μSR is a unique technique for the study of local magnetic properties at arbitrarily low magnetic fields.[19,20] We have also carried out transverse-field (TF) μSR (muon spin perpendicular to applied field) in $YbRh_2Si_2$ at higher fields and temperatures in order to characterize the local magnetic susceptibility and its inhomogeneity. Preliminary reports of some of this work[21,22] have been submitted for publication. ^{29}Si NMR studies have also been performed in $YbRh_2Si_2$ as noted above[16] but, due to the low natural isotopic abundance of ^{29}Si (4.8%) and consequent low signal-to-noise ratio, to date NMR measurements have only been performed above $\sim$1.5 kOe.

Elements of the ZF-, LF-, and TF-μSR techniques used in this study are briefly reviewed in Secs. I and I A, respectively. In Sec. II we describe our experimental results on $YbRh_2Si_2$, which include the temperature dependence of the ZF muon relaxation, the field dependence of LF relaxation at 20 mK, the temperature dependence of the muon spin relaxation rate at a longitudinal field $H_L = 19$ Oe, and temperature dependence of the average $K_{\rm av}$ and r.m.s. width $\delta K_{\rm r.m.s.}$ of the muon Knight shift distribution from TF-μSR measurements above 2 K. The implications of these results for the magnetic state below the 70-mK transition and the spin dynamics at low temperatures and fields are discussed in Sec. III. In this section we also consider the implanted muon stopping site using the $K_{\rm av}$ and $\delta K_{\rm r.m.s.}$ data together with the bulk anisotropic susceptibility measured on a single crystal. The present μSR and ^{29}Si NMR data at low temperatures are also compared in Sec. III. Finally, we summarize our results in Sec. IV. Determination of the probable muon stopping site from TF-μSR data is described in the Appendix.

A. Zero- and longitudinal-field muon spin rotation (ZF- and LF-μSR)

μSR is a sensitive local probe of static and dynamic magnetism in solids.[23,24] Spin-polarized positive muons (μ^+) are implanted into the sample, and the subsequent decay of the μ^+ spin polarization is monitored in time by measuring the asymmetry in the number of decay positrons emitted parallel and antiparallel to the μ^+ spin direction. The resulting relaxation function $G(t)$ is analogous to the free induction signal in a pulsed NMR experiment. An advantage of μSR compared with NMR is that the former can be performed in zero and weak applied magnetic fields, whereas NMR requires a substantial applied field. The shape and duration of $G(t)$ are influenced by the local magnetic fields at the μ^+ stopping sites due to their magnetic environments.

There are two classes of relaxation mechanisms. Relaxation by a distribution of static local fields reflects a spatial distribution of μ^+ Larmor precession frequencies and hence of the local fields. Then $G(t)$ relaxes due to loss of phase coherence between processing μ^+ spins, and the relaxation time is of the order of the inverse of the spread in Larmor frequencies. If the μ^+ local field distribution is due to randomly oriented neighboring magnetic dipole moments (nuclear or electronic), the central limit theorem suggests a Gaussian field distribution if more than a few moments contribute, in which case $G(t)$, which is the Fourier transform of the frequency distribution, is also Gaussian. Fields due to randomly oriented nuclear dipolar moments, which usually do not reorient on the time scale of μSR experiments, often give rise to static relaxation.[25]

ZF-μSR is also a very good probe of static electronic magnetism, with or without long-range order. Although ZF-μSR, unlike neutron diffraction, gives little or no information on the magnetic structure, it is extremely sensitive to weak magnetism: moments of the order of $10^{-3}\mu_B$ produce observable static relaxation.

Dynamic μ^+ local fields due to thermally excited spin fluctuations lead to spin-lattice relaxation, as in NMR, and as in the latter case the relaxation rate is a measure of the spectral density of the fluctuations at the (low) muon or nuclear Zeeman frequency. In the case of dynamic relaxation $G(t)$ often shows exponential behavior.

Static and dynamic relaxation mechanisms can be distinguished by μSR experiments in a longitudinal applied magnetic field $\mathbf{H}_L$ (i.e., a field parallel to the μ^+ spin direction) much larger in magnitude than a typical local field $\mathbf{B}_{\rm loc}$. This produces a resultant field $\mathbf{H}_L + \mathbf{B}_{\rm loc}$ essentially in the direction of the applied field and hence of the μ^+ spin. If $\mathbf{H}_L + \mathbf{B}_{\rm loc}$ is static the muons do not precess substantially, and their spin polarization is maintained indefinitely. This procedure is known as ''decoupling'' of the μ^+ spin. The expected field for decoupling is a few times the spread $\Delta B_{\rm loc}$ in local fields, which can be estimated self-consistently by assuming that the relaxation is static. Then the observed relaxation rate gives the spread $\gamma_\mu \Delta B_{\rm loc}$ of μ^+ precession frequencies, where $\gamma_\mu = 2\pi \times 13.554$ kHz G^{-1} is the μ^+ gyromagnetic ratio, and decoupling is complete for $H_L \gg \Delta B_{\rm loc}$. If on the other hand the relaxation is dynamic (i.e., due to thermal fluctuation of $\mathbf{B}_{\rm loc}$), then the relaxation rate is usually much less affected by the relatively weak applied field (typically $H_L \lesssim 100$ Oe) required for decoupling.

ZF- and LF-μSR relaxation data are often analyzed using the Kubo-Toyabe (KT) model,[25] which treats the distribution and dynamical fluctuation of $\mathbf{B}_{\rm loc}$. This model determines the shape of the relaxation function and its rate of decay as a function of $\mathbf{H}_L$ and the parameters that characterize $\mathbf{B}_{\rm loc}$. Experimental ZF- and LF-μSR data for $YbRh_2Si_2$ are discussed in Sec. II.

B. Transverse-field muon spin rotation (TF-μSR)

In TF-μSR one measures the Larmor precession of the μ^+ spin under the influence of the static magnetic field at the μ^+ stopping site in the crystal lattice. The precession frequency is given by $\gamma_\mu B_\mu$, where B_μ is the total magnetic field at the μ^+ stopping site, i.e., the sum of the external field and the internal field at the μ^+ stopping site. Neglecting the diamagnetic and Pauli paramagnetic fields, the total field at the μ^+ stopping site in $YbRh_2Si_2$ is given by $\mathbf{B}^\mu = \mathbf{H}_{\rm ext} + \mathbf{B}^{\rm hf}$, where $\mathbf{H}_{\rm ext}$ is the externally applied field and $\mathbf{B}^{\rm hf}$ is the transferred hyperfine field originating from the polarization of the Yb^{3+} $4f$ moments. In the following discussion the Lorentz and demagnetization fields are included in $\mathbf{H}_{\rm ext}$ for simplicity.

The polarization of the Yb^{3+} moments affects the field at the μ^+ stopping site through two coupling mechanisms: the direct dipolar field at the interstitial μ^+ stopping site, and polarization of the conduction electrons by the Yb^{3+} moments, which produces an additional field at the μ^+ stopping site by the indirect Ruderman-Kittel-Kasuya-Yosida (RKKY) mechanism. The field produced by both dipolar and RKKY fields is proportional to the field-induced Yb^{+3} atomic magnetic moment $\boldsymbol{\mu}_f$:

$$\mathbf{B}^{\rm hf} = \mathbf{A}^{\rm hf} \cdot \boldsymbol{\mu}_f = \mathbf{A}^{\rm hf} \cdot \boldsymbol{\chi}_f \cdot \mathbf{H}_{\rm ext}, \tag{1}$$

where $\mathbf{A}^{\rm hf}$ is the hyperfine coupling field tensor at the μ^+ stopping site and $\boldsymbol{\chi}_f$ is the Yb^{3+}-moment susceptibility tensor. Thus $\mathbf{A}^{\rm hf}$ can be decomposed into dipolar and RKKY terms $\mathbf{A}^{\rm hf} = \mathbf{A}^{\rm dip} + \mathbf{A}^{\rm RKKY}$. The dipolar term is a tensor given by

$$\mathbf{A}^{\rm dip} = \sum_{\mathbf{r}} \left(\frac{3\hat{\mathbf{r}}\cdot\hat{\mathbf{r}} - \mathbf{1}}{r^3} \right), \tag{2}$$

where the summation extends over the Yb^{3+} moments in a Lorentz sphere, $\mathbf{r} = (x_1, x_2, x_3)$ are vectors from the muon to each of the moments included in the summation, $\hat{\mathbf{r}}$ is a unit vector in the direction of $\mathbf{r}$, and $\mathbf{1}$ is the unit tensor ($\mathbf{1}_{ij} = \delta_{ij}$). The dipolar contribution is especially important for the determination of the μ^+ stopping site. There is no simple expression for $\mathbf{A}^{\rm RKKY}$, but if we reasonably assume that the coupling through the conduction electrons is isotropic in nature then $\mathbf{A}^{\rm RKKY} = A^{\rm RKKY}\mathbf{1}$. This assumption, together with lattice-sum calculations of $\mathbf{A}^{\rm dip}$ for various candidate μ^+ stopping sites[26] [Eq. (2)], allows determination of the probable site.

The Yb^{3+}-moment Knight shift tensor $\mathbf{K}$ is defined by

$$\mathbf{B}^\mu \equiv (\mathbf{1} + \mathbf{K}) \cdot \mathbf{H}_{\rm ext} \tag{3}$$

so that $\mathbf{K}$, given by

$$\mathbf{K} = \mathbf{A}^{\rm hf} \cdot \boldsymbol{\chi}_f, \tag{4}$$

expresses the relative frequency shift at the μ^+ stopping site. For a given direction of $\mathbf{H}_{\rm ext}$ the shifted resonance frequency ω is given by

$$\omega = \omega_0 (1 + K), \tag{5}$$

where $\omega_0 = \gamma_\mu H_{\rm ext}$ and to first order in K

$$K = \frac{\mathbf{H}_{\rm ext} \cdot (\mathbf{B}^\mu - \mathbf{H}_{\rm ext})}{H_{\rm ext}^2} = \hat{\mathbf{H}}_{\rm ext} \cdot \mathbf{K} \cdot \hat{\mathbf{H}}_{\rm ext}; \tag{6}$$

here $\hat{\mathbf{H}}_{\rm ext}$ is a unit vector in the direction of $\mathbf{H}_{\rm ext}$.

In a randomly oriented powder sample K given by Eq. (6) is distributed. Then the angular (''powder'') average $K_{\rm av}$ and r.m.s. spread $\delta K_{\rm r.m.s.}$ of this distribution are directly related to the TF-μSR shift and relaxation rate, respectively. More specifically, the Knight shift (including the RKKY term) in a single crystal (i.e., a powder grain) is given by

$$K(\hat{\mathbf{H}}_{\rm ext}) = K_{11}\gamma_1^2 + K_{22}\gamma_2^2 + K_{33}\gamma_3^2, \tag{7}$$

where $(\gamma_1, \gamma_2, \gamma_3)$ are the direction cosines of $\hat{\mathbf{H}}_{\rm ext}$ relative to the principal axes of $\boldsymbol{K}$. Then the angular average is

$$K_{\rm av} = \frac{1}{3}(K_{11} + K_{22} + K_{33}), \tag{8}$$

where the angular averages $(\gamma_i^2)_{\rm av} = 1/3$ have been used. The difference $\delta K(\hat{\mathbf{H}}_{\rm ext}) = K(\hat{\mathbf{H}}_{\rm ext}) - K_{\rm av}$ is then

$$\delta K(\hat{\mathbf{H}}_{\rm ext}) = K_{11}\left(\gamma_1^2 - \frac{1}{3}\right) + K_{22}\left(\gamma_2^2 - \frac{1}{3}\right) + K_{33}\left(\gamma_3^2 - \frac{1}{3}\right), \tag{9}$$

and $\delta K_{\rm r.m.s.}$ is given by

$$(\delta K_{\rm r.m.s.})^2 = \frac{4}{45}(K_{11}^2 + K_{22}^2 + K_{33}^2 - K_{11}K_{22} - K_{22}K_{33} - K_{33}K_{11}), \tag{10}$$

where the angular averages $(\gamma_i^2\gamma_j^2)_{\rm av} = (2\delta_{ij} + 1)/15$ have been used. In Sec. III B and the Appendix Eqs. (8) and (10), together with experimental values of the mean and r.m.s. width of the Yb^{3+}-moment Knight shift distribution (Sec. I A), are used to determine the most probable muon stopping site.

II. EXPERIMENTAL RESULTS

A powder sample of small-grain single crystals of $YbRh_2Si_2$ was used for the present μSR experiments, since preparing a large single crystal is so difficult in this compound. This sample was taken from the same batch used for the ^{29}Si NMR experiments.[16] Bulk properties such as the resistivity, specific heat and susceptibility down to 10 mK have been reported.[14,18] Small-grain samples of $\sim$1 g were pressed with GE 7031 varnish into pellets 13 mm diameter

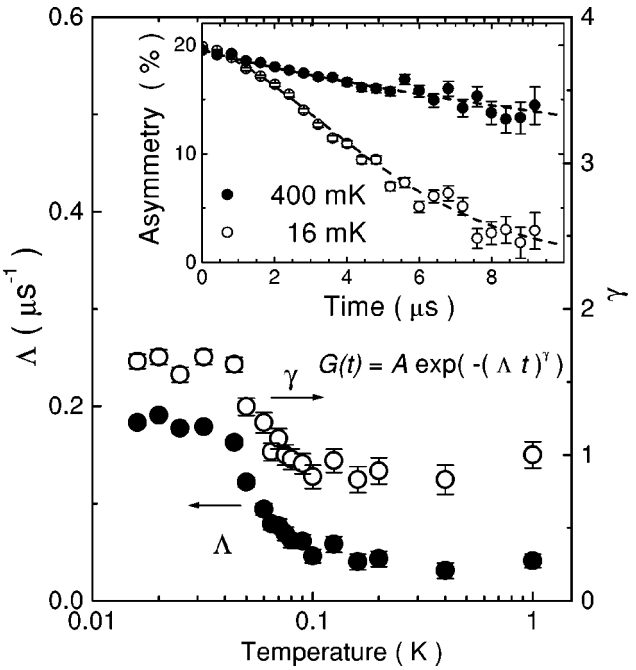

FIG. 1. Temperature dependence of the zero-field μ^+SR relaxation rate Λ (solid circles) and exponent γ (open circles) in $YbRh_2Si_2$ from fits of the power-exponential function $G(t)=A\exp[-(\Lambda t)^{\gamma}]$ to ZF-μSR relaxation data. Inset: zero-field μ^+SR asymmetry relaxation functions $G(t)$ in $YbRh_2Si_2$ at 400 and 16 mK. Dotted lines: fits to the power exponential form $G(t)=\exp[-(\Lambda t)^{\gamma}]$.

$\times 1$ mm thickness and were attached onto a silver sample holder. μSR experiments were carried out at the πM3 beam line of the Paul Scherrer Institute (PSI), Villigen, Switzerland. TF-μSR data were obtained above 2 K in an external magnetic field $H_{\rm ext}=6$ kOe using the PSI General Purpose Spectrometer, and ZF- and LF-μSR data were taken for temperatures between 16 and 1100 mK in the PSI Low Temperature Facility. ZF- and LF-μSR experiments were also performed down to 20 mK at the low-temperature facilities at KEK in Tsukuba, Japan. ZF- and LF-μSR data taken at two facilities were consistent with each other. Experimental data obtained at PSI are reported in this article, and LF-μSR data in the higher temperature range up to 2 K, which were obtained at KEK, are also shown.

A. ZF-μSR experiments

The inset of Fig. 1 shows the time dependence of the ZF-μSR muon decay asymmetry at 400 and 16 mK; the time dependence of the asymmetry gives the ZF-μSR relaxation function $G(t)$.[23,24] The relaxation is much faster at 16 mK, and the functional form of $G(t)$ at 16 mK appears to differ from that at 400 mK. The relaxation rate at 16 mK is too slow for the static KT recovery of the μ^+ polarization to $G(t\rightarrow\infty)=1/3$ (Ref. 25) to be observed within the time window of the present experiment.

The experimental asymmetry data were fit to the ''power exponential'' form

$$G(t)=A\exp[-(\Lambda t)^{\gamma}], \tag{11}$$

where A is the initial muon decay asymmetry, Λ is a generalized relaxation rate, and the exponent γ interpolates between exponential ($\gamma=1$) and Gaussian ($\gamma=2$) limits. We employed this fitting formula because its parameters give a crude indication of the behavior of the relaxation, i.e., whether the relaxation is exponential (i.e., probably dynamic), Gaussian (i.e., probably static), or intermediate between these limits.

The parameters Λ and γ are plotted versus temperature in the main panel of Fig. 1. Both parameters are independent of temperature in the range 0.1–1 K, and increase with decreasing temperature below 70 mK. The value $\gamma\approx 1$ found above 100 mK indicates that the behavior of the relaxation is exponential in this range. This is in contrast to the behavior of the KT relaxation function (which is Gaussian for short times) that characterizes relaxation due solely to static nuclear dipolar fields. Above 100 mK the exponential behavior suggests dynamical relaxation, as discussed in Sec. III C. The constant value of $\Lambda\approx 0.041\ \mu s^{-1}$ in this temperature range is, however, of the same order as the (Gaussian) nuclear dipolar rate, as discussed in Sec. III B.

Both Λ and γ increase below 70 mK and level off below 40 mK. The increase of γ suggests a crossover from a dynamic to nearly static relaxation behavior at low temperatures, indicating Yb^{3+}-moment freezing below ~ 70 mK. The entire μ^+ relaxation function is characterized by this static relaxation, consistent with Yb^{3+}-moment freezing over the entire sample volume; the data put an upper limit of a few percent on any coexisting paramagnetic volume fraction. The low-temperature value $\gamma\approx 1.6$ indicates that the relaxation rate is nearly but not quite Gaussian, suggesting that dynamical relaxation coexists with dominant static relaxation.

The spread in internal field at μ^+ stopping sites is estimated from the relaxation rate at the lowest temperature to be ~ 2 G. The magnitude of the static Yb^{3+} moment that gives rise to this field depends on the μ^+ stopping site, as discussed in Sec. III B, but in any event is quite small. The dynamical relaxation observed at low temperatures in LF decoupling experiments is analyzed in Sec. III C below.

B. LF-μSR experiments

LF-μSR measurements have been carried out in longitudinal field H_L under the same conditions as the ZF-μSR measurements. The inset of Fig. 2 shows $G(t)$ for $H_L=0$, 11, 28, and 100 Oe at $T=20$ mK. The relaxation functions for all applied fields except zero field can be fit to an exponential function $G(t)=A\exp(-t/T_1)$. This functional form indicates that the relaxation rate is spatially uniform over the sample, since in general a distribution of rates leads to a sample-average $G(t)$ that varies more slowly than exponentially,[27,13] and is evidence against a disorder-driven mechanism for the NFL behavior of $YbRh_2Si_2$. Further evidence for this view obtained from TF-μSR experiments is discussed in Sec. III A.

The main panel of Fig. 2 shows the dependence of the LF-μSR relaxation rate $1/T_1$ on longitudinal field at 20 mK. The relaxation rate shows a weak field dependence for H_L

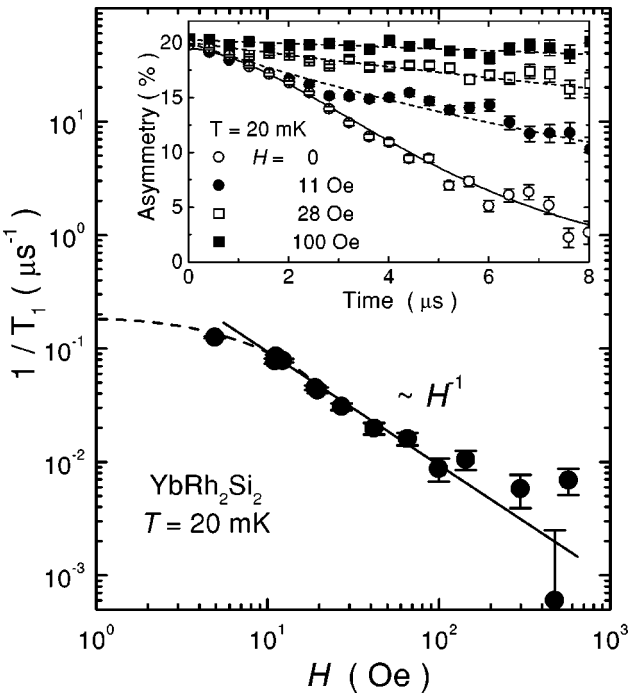

FIG. 2. Longitudinal field dependence of LF-μSR relaxation rate $1/T_1$ in $YbRh_2Si_2$ at $T=20$ mK. Inset: ZF- and LF-μSR relaxation in $YbRh_2Si_2$ measured at $T=20$ mK in external magnetic fields $H=0$, 11, 28, and 100 Oe. Solid curve: power-exponential fit for $H_L=0$ (cf. inset of Fig. 1). Dotted curves: exponential fits for $H_L>0$.

$\lesssim$10 Oe but varies more strongly, as H_L^{-1}, for $H_L \gtrsim 20$ Oe. It should be noted that 20 Oe, which is nearly 10 times larger than the estimated static internal field below 70 mK, is large enough for decoupling. The field dependence of $1/T_1$ above 20 Oe is therefore not due to decoupling, and instead indicates a field dependence of the dynamic relaxation mechanism.

Figure 3 gives the temperature dependence of $1/T_1$ for $H_L=19$ Oe. Data below 0.25 K were obtained at PSI, and data between 0.09 and 2 K were obtained at KEK. The results are consistent in the temperature range between 0.09 and 0.25 K. It can be seen that $1/T_1$ shows a weak temperature dependence that can be fit to a $-\ln T$ law above the Néel temperature $T_N=70$ mK. A small anomaly in $1/T_1$ is seen below T_N that contrasts with the usual behavior of $1/T_1$ in the neighborhood of a magnetic transition, i.e., a maximum at T_N due to critical slowing down of magnetic fluctuations. The smallness of the anomaly in $1/T_1$ is, however, consistent with other bulk measurements that show only weak changes at the transition; the resistive anomaly is only seen in high-purity samples, and the entropy release at T_N is very small, only about $0.01R \ln 2$.[15,17,18] These results suggest that magnetic fluctuations are relatively unaffected by the transition, and the continuous increase of $1/T_1$ down to the lowest temperatures also suggests that critical magnetic fluctuations related to the QCP are present even below T_N. The inset to Fig. 3 shows that the data can also be fit to a weak power-law ($T^{-0.17\pm0.03}$) temperature dependence over more than a decade of temperature variation. Properties of the magnetic

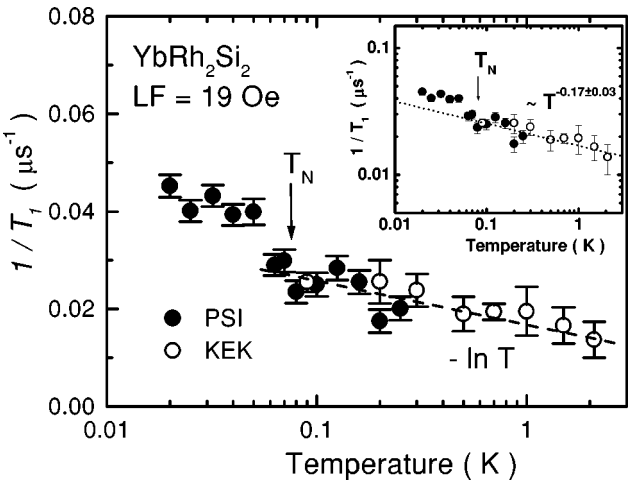

FIG. 3. Temperature dependence of $1/T_1$ in $YbRh_2Si_2$ for $H_L=19$ Oe. Filled circles: data obtained at PSI. Open circles: data obtained at KEK. T is plotted on a log scale. Inset: same data, with $1/T_1$ and T plotted on log scales.

fluctuations at low temperatures are discussed below in Sec. III C in relation to the spectral density of the fluctuations.

C. TF-μSR experiments

TF-μSR spectra were obtained for applied field $H_{\rm ext}=6$ kOe over the temperature range 1.8–250 K. It was found that the TF-μSR relaxation function is approximately exponential over this temperature range as shown in Fig. 4, where the oscillatory factor is removed by transforming to a reference frame rotating at the μ^+ precession frequency. In this case the exponential relaxation is not dynamic in origin, but reflects an approximately Lorentzian distribution of precession frequencies. The slight Gaussian-like behavior at early times for $T=250$ K may be due to the emergence of the nuclear dipolar component as the Yb^{3+} moment broadening decreases at high temperatures.

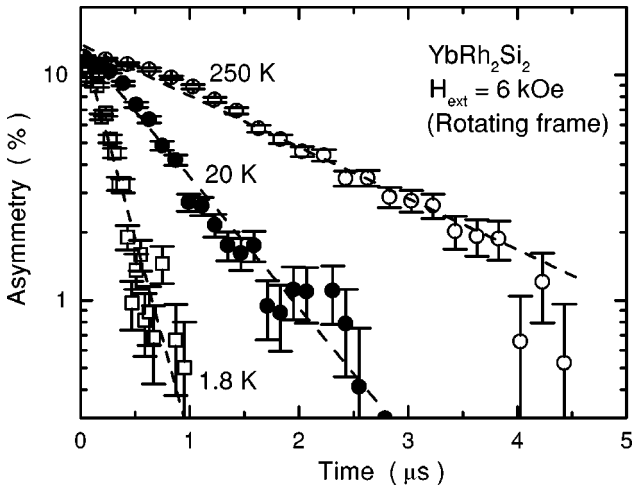

FIG. 4. Semilog plot of TF-μSR asymmetry relaxation function in $YbRh_2Si_2$ (after transformation to a reference frame rotating with the μ^+ precession frequency). Straight lines: exponential fits.

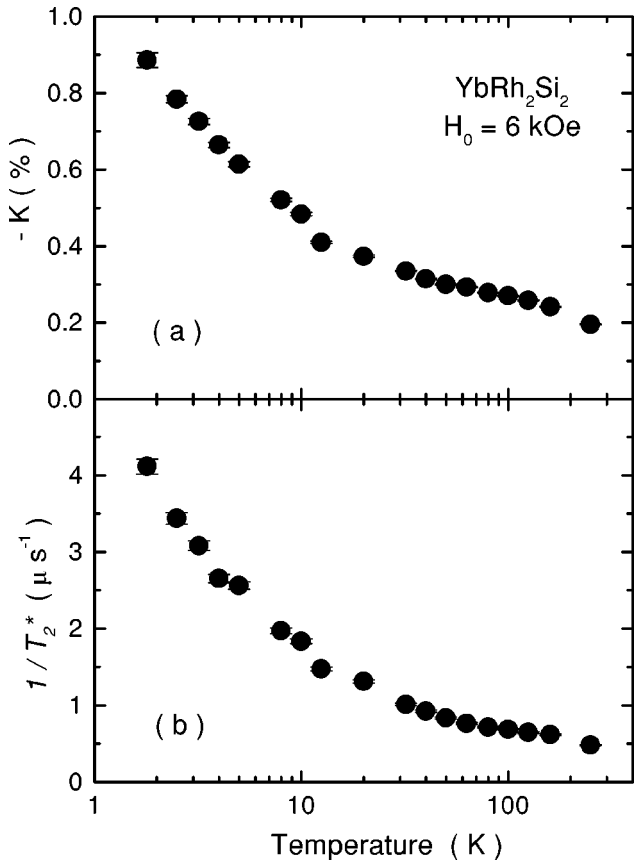

FIG. 5. Temperature dependence of μ^+ (a) frequency shift K and (b) relaxation rate $1/T_2^*$ in $YbRh_2Si_2$.

Average frequency shifts K and exponential relaxation rates $1/T_2^*$ were obtained from fits of the data to the relaxation function

$$G(t)=A\exp(-t/T_2^*)\cos[\gamma_\mu H_{\rm ext}(1+K)t+\phi], \quad (12)$$

where A is the initial muon decay asymmetry and ϕ is the phase of the initial μ^+ spin orientation. The temperature dependence of K and $1/T_2^*$ at 6 kOe are shown in Fig. 5. Both quantities increase considerably in magnitude with decreasing temperature.

In general $1/T_2^*$ is due to a combination of the dynamics of the internal fields (lifetime broadening) and the dephasing due to a static distribution of Larmor frequencies. As discussed in Sec. II B, the LF-μSR data indicate that fields greater than 500 Oe are enough to suppress $1/T_1$, and in any event the observed data yield $1/T_1 \ll 1/T_2^*$. Thus $1/T_2^*$ is dominated by static inhomogeneous line broadening, related to the spread δK of the Knight shift by the relation $\delta K = 1/(\gamma_\mu H_{\rm ext} T_2^*)$. We argue in Sec. III that this linewidth is mainly due to powder-pattern broadening arising from the anisotropic Knight shift and the randomly oriented powder grains of the sample.

Both K and δK are accurately proportional to the sample-average bulk susceptibility $\chi_{\rm av}=(\chi_a+\chi_b+\chi_c)/3$ (except perhaps at the lowest temperatures) as shown in Fig. 6. From

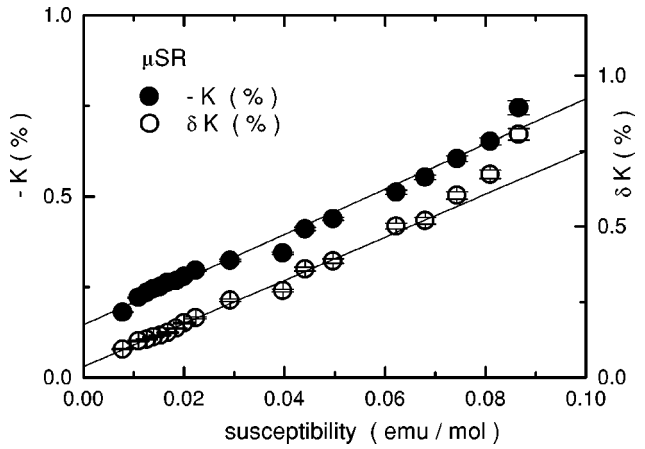

FIG. 6. Dependence of K and δK on bulk susceptibility χ in $YbRh_2Si_2$, with temperature an implicit parameter.

the slopes, the average $A_{\rm av}^{\rm hf}=N_A\mu_B K/\chi_{\rm av}$ and inhomogeneous spread $\delta A_{\rm r.m.s.}^{\rm hf}=N_A\mu_B\delta K/\chi_{\rm av}$ in hyperfine coupling fields are found to be

$$A_{\rm av}^{\rm hf}=-349\pm 12 \ \ {\rm G}/\mu_B \quad (13)$$

and

$$\delta A_{\rm r.m.s.}^{\rm hf}=399\pm 11 \ \ {\rm G}/\mu_B, \quad (14)$$

respectively. We note that the intercept $K(\chi=0)$ in Fig. 6, which arises from sources other than Yb^{3+} moments (e.g., the Knight shift due to the conduction-electron Pauli susceptibility), is appreciable.

We discuss below the possibility that K and δK are related to the spatially inhomogeneous susceptibility postulated in disorder-driven mechanisms for NFL behavior.[28–30] We also consider the alternative that K and δK arise from powder averages, and how under this assumption the coupling constants $A_{\rm av}^{\rm hf}$ and $\delta A_{\rm r.m.s.}^{\rm hf}$ can be used in the assignment of the μ^+ stopping site (Sec. III B).

III. DISCUSSION

We first compare the behavior of $K_{\rm av}$ and $\delta K_{\rm r.m.s.}$ to that expected from the disorder-driven NFL mechanisms.[28–30] Experimental results for the ^{29}Si NMR linewidth are also shown and compared with the present μSR results in Sec. III A. In Sec. III B we discuss determination of the implanted μ^+ stopping site, which is important for the estimation of the magnitude of the ordered Yb^{3+} moment below T_N, using TF-μSR data. Finally, the spin dynamics at low temperatures are discussed in Sec. III C.

A. Relation between μSR/NMR linewidth and susceptibility

Strong temperature-dependent inhomogeneity of the spin susceptibility has been shown to be a signature of disorder-driven contribution to the NFL behavior in a number of NFL alloys.[28] In $UCu_{5-x}Pd_x$, $x=1.0$ and 1.5 (Refs. 28 and 31) and $CeRhRuSi_2$ (Refs. 32 and 33), NMR and μSR experiments revealed a strong temperature dependence and large

low-temperature values of the inhomogeneous resonance linewidth compared with the average shift, suggestive of a broad distribution of the local static susceptibilities. This inhomogeneity effect can be understood in the so-called ''Kondo-disorder'' model of Bernal *et al.*[28] and Miranda, Dobrosavljević, and Kotliar,[29] which attributes the susceptibility inhomogeneity to a disordered spatial distribution of Kondo temperatures T_K, and also in the Griffiths-singularity cluster model of Castro Neto, Castilla, and Jones.[30] It is important to determine whether such a disorder-driven NFL mechanism is present in the stoichiometric NFL compound $YbRh_2Si_2$, since stoichiometry by itself does not ensure long-range structural order; for example, stoichiometric UCu_4Pd exhibits disorder due to Pd-Cu site interchange.[34] μSR and NMR resonance linewidths, which arise from the distribution of the Knight shifts, are useful in determining the microscopic distribution of the local susceptibility. In the following we briefly outline how μSR and NMR resonance linewidths give evidence concerning the origin of this distribution.[28]

In the simplest case the local Knight shift is given by $K(\mathbf{r})=a(\mathbf{r})\chi(\mathbf{r})$, where the hyperfine coupling $a(\mathbf{r})$ and the local susceptibility $\chi(\mathbf{r})$ may both be spatially nonuniform. If the distributions of these quantities are uncorrelated the average $\overline{K}$ of the Knight shift can be written as $\overline{K}=\overline{a\chi}=(\overline{a})(\overline{\chi})$ (the overline indicates a spatial average). Similarly, the r.m.s. width $\kappa=\delta K_{\text{r.m.s.}}\equiv[\overline{K^2}-(\overline{K})^2]^{1/2}$ of the Knight shift distribution is given by

$$\kappa=\delta(a\chi)_{\text{r.m.s.}}. \tag{15}$$

For uncorrelated distributions of a and χ, κ divided by the magnitude $|\overline{K}|$ of the average Knight shift is approximately given by

$$\frac{\kappa}{|\overline{K}|}\approx\sqrt{\left(\frac{\delta\chi_{\text{r.m.s.}}}{\overline{\chi}}\right)^2+\left(\frac{\delta a_{\text{r.m.s.}}}{\overline{a}}\right)^2}. \tag{16}$$

Thus $\kappa/|\overline{K}|$ is a measure of the fractional spread in susceptibility if the latter is greater than the fractional spread in a.

A simple heuristic model shows how $\delta\chi_{\text{r.m.s.}}/\overline{\chi}$ (and hence $\kappa/\overline{K}$) might increase at low temperatures. In both the Kondo-disorder and Griffiths-singularity models the local susceptibility $\chi(T)$ is assumed to follow a Curie-Weiss temperature dependence $\chi(T)\propto 1/(T+\Delta)$, where Δ is a characteristic energy (Kondo temperature in the Kondo-disorder model, cluster tunneling energy in the Griffiths-singularity picture) that is distributed. Then if this distribution is not too wide $\delta\chi_{\text{r.m.s.}}$ can be written $\delta\chi_{\text{r.m.s.}}\approx|\partial\chi/\partial\Delta|\,\delta\Delta_{\text{r.m.s.}}\propto\chi^2$ for fixed $\delta\Delta_{\text{r.m.s.}}$, so that $\delta\chi_{\text{r.m.s.}}/\chi$ varies linearly with χ, as does $\kappa/|\overline{K}|$ if $\delta a_{\text{r.m.s.}}$ does not contribute significantly. If on the other hand $\delta\chi_{\text{r.m.s.}}$ is small, then $\kappa/|\overline{K}|$ is dominated by $\delta a_{\text{r.m.s.}}$. This is determined by the temperature-independent hyperfine coupling, so that both κ and $|\overline{K}|$ are proportional to χ and $\kappa/|\overline{K}|\approx$const.

NMR and μSR experiments on $UCu_{5-x}Pd_x$, $x=1.0$ and 1.5 (Refs. 28 and 31) found considerable temperature dependence of $\kappa/|\overline{K}|$, which is roughly proportional to χ and grows to large values (~ 2) at low temperatures. These experimental results are in good agreement with disorder-driven NFL models and give clear evidence for susceptibility inhomogeneity, which suggests that a disorder-driven mechanism contributes to NFL behavior in $UCu_{5-x}Pd_x$.

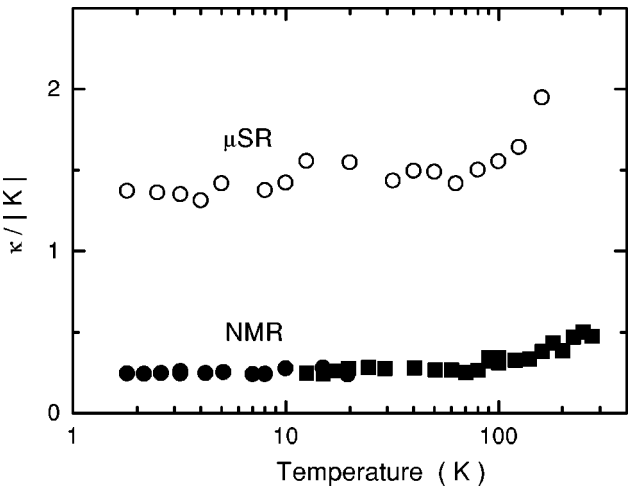

FIG. 7. Temperature dependence of $\delta K/|K|$ in $YbRh_2Si_2$ from μSR and NMR measurements, with temperature an implicit parameter. Unaligned and aligned powder samples were used for μSR and NMR, respectively. In the NMR data the solid squares and circles are measured at 20.5 MHz ($\sim$24.4 kOe) and 8.6 MHz ($\sim$10.0 kOe), respectively.

Figure 7 gives the temperature dependence of $\kappa/|K|$ ($K=K_{\text{av}}$) in $YbRh_2Si_2$ from the present μSR data and also from ^{29}Si NMR measurements, which were performed using a field-aligned powder sample with the crystalline ab plane parallel to the external field. It can be seen that $\kappa/|K|$ from both measurements exhibits very little temperature dependence below $\sim$70 K down to 1.8 K$\ll T_K\approx$25 K. This contrasts with the behavior observed in disorder-driven NFL systems, and suggests that in $YbRh_2Si_2$ the susceptibility is essentially uniform. The lack of magnetic disorder in $YbRh_2Si_2$ is consistent with a low level of structural disorder, as evidenced by the small residual resistivity $\rho_0\approx 1.0\ \mu\Omega$ cm (Ref. 18) of this compound.

The value of $\kappa/|K|$ from μSR is five times larger than that from ^{29}Si NMR. This discrepancy appears to be mainly due to differences in experimental circumstances, since the μSR was performed on a randomly oriented powder sample whereas the NMR experiments utilized a field-aligned powder sample. The large difference of the magnitude between NMR and μSR strongly suggests that the anisotropic Knight shift, rather than disorder-induced spatial inhomogeneity, dominates the linewidth in the μSR experiments. Shift anisotropy is discussed in connection with the μ^+ stopping site in the next section.

We conclude that disorder-driven NFL is not a major factor in the NFL behavior of stoichiometric $YbRh_2Si_2$. A promising NFL mechanism suggested by a recent NMR study[16] is introduced briefly in Sec. III C.

TABLE I. Calculated powder-average ZF-μSR static Gaussian relaxation rate σ_{ZF} for candidate μ^+ stopping sites (multiplicity, Wyckoff letter, and relative coordinates in the bct lattice) in $YbRh_2Si_2$. Contributions from ^{171}Yb, ^{173}Yb, ^{103}Rh, and ^{29}Si nuclei have been included. The observed value of the exponential relaxation rate above 70 mK (Fig. 1) is also given for comparison.

site	σ_{ZF} (μs^{-1})
$2b[\frac{1}{2},\frac{1}{2},0]$	0.040
$4c[\frac{1}{2},0,0]$	0.021
$4e(0,0,\frac{1}{4}]$	0.031
$4e[\frac{1}{2},\frac{1}{2},\frac{5}{16}]$	0.020
$8f[\frac{1}{4},\frac{1}{4},\frac{1}{4}]$	0.023
$8g(0,\frac{1}{2},\frac{1}{8}]$	0.026
$8g[\frac{1}{2},0,\frac{1}{16}]$	0.020
$8j[\frac{1}{2},\frac{1}{4},0]$	0.023
$16m[\frac{1}{4},\frac{1}{4},\frac{5}{32}]$	0.024
$16m[\frac{1}{8},\frac{1}{8},\frac{7}{32}]$	0.021
$16n[\frac{1}{8},\frac{1}{2},\frac{3}{32}]$	0.022
Experimental (exponential)	0.04 ± 0.01

B. Probable μ^+ stopping site; static Yb^{3+} moment below 70 mK

Determination of the μ^+ stopping site, which is a basic issue in μSR experiments, can be quite difficult when a number of possible stopping sites are present in a compound. A number of possible μ^+ stopping sites for the $YbRh_2Si_2$ crystal structure[26] (space group $I4/mmm$) are listed in Table I. [The site notation indicates site multiplicity, Wyckoff letter, and relative coordinates in the body-centered tetragonal (bct) unit cell.]

Two methods that are commonly used to determine the μ^+ stopping site in *f*-ion systems[19] involve comparison of calculated and measured quantities that depend on the site environment. These methods use (1) the zero-field KT nuclear dipolar relaxation rate and (2) the anisotropic Knight shift due to dipolar fields at the μ^+ stopping site from Yb^{3+} moments. We consider these methods in turn.

In $YbRh_2Si_2$ all constituent atoms have isotopes with a nuclear dipole moment: ^{171}Yb, ^{173}Yb, ^{103}Rh, and ^{29}Si. The calculated μ^+ ZF relaxation rates σ_{ZF} due to dipolar coupling to these nuclei at candidate μ^+ stopping sites are given in Table I. The observed relaxation rate in the paramagnetic region above 70 mK is comparable to but greater than the calculated nuclear dipole contribution. The observed relaxation function is exponential, however, which suggests the importance of spin dynamics in the ZF relaxation process. Furthermore, static dipolar relaxation rates much smaller than 0.04 μs^{-1} would not be measurable in the presence of the observed exponential relaxation. Thus it is not possible to identify the μ^+ stopping site solely from the nuclear dipole field, because the calculated KT relaxation rates of Table I are all smaller than the observed exponential rate.

We therefore use the anisotropy of the shift to identify potential μ^+ stopping sites, noting that in *f*-electron systems the anisotropic shift is typically dominated by the f-μ^+ dipolar interaction.[19] Our sample was an unaligned powder, so we are not able to measure this anisotropy directly. Instead, we attribute the width of the μ^+ line to powder-pattern broadening, and use the average K_{av} and r.m.s. width $\delta K_{r.m.s.}$ of the Knight shift distribution (Fig. 6). In the Appendix experimental values of K_{av} and $\delta K_{r.m.s.}$ from Sec. I A are used to obtain estimates for elements of the dipolar coupling field tensor $\mathbf{A}^{dip}$ for specific point symmetries of this tensor. These elements are then compared with lattice-sum calculations of $\mathbf{A}^{dip}$ at the candidate μ^+ stopping sites considered above (Table I).

The $4e[\frac{1}{2},\frac{1}{2},\frac{5}{16}]$ site (or, equivalently, the $4e[0,0,\frac{3}{16}]$ site) is found to be the most probable μ^+ stopping site. This differs from results for μ^+ stopping sites in two Ce compounds with the same $ThCr_2Si_2$ structure;[19] in $CeRu_2Si_2$ the $2b[\frac{1}{2},\frac{1}{2},0]$ site was obtained from the anisotropy of the hyperfine coupling constants in a single crystal,[35] and in $CeRh_2Si_2$ the $4c[\frac{1}{2},0,0]$ site was found from an analysis of the internal field below the Néel temperature.[36] These latter two sites are in the Ce layer. On the other hand, the $4e[\frac{1}{2},\frac{1}{2},\frac{5}{16}]$ site for $YbRh_2Si_2$ is close to the $[0,0,0.20]$ μ^+ stopping site reported in tetragonal $HoNi_2B_2C$.[37]

From ZF-μSR experiments we find that a static magnetic field $H_{stat}\approx 2$ G due to frozen Yb^{3+} moments is induced at the μ^+ stopping site at 16 mK (Sec. II A). To estimate the static Yb^{3+} moment μ_{stat} responsible for this field an ordered AFM structure is assumed as an example; we calculate H_{stat} for the structure observed in $CePd_2Si_2$, where the magnetic moments are oriented in the $[1,1,0]$ direction with a propagation vector $\mathbf{Q}=(\frac{1}{2},\frac{1}{2},0)$. When the muon is assumed to stop at the $4e[\frac{1}{2},\frac{1}{2},\frac{5}{16}]$ site in $YbRh_2Si_2$ the dipolar field at the μ^+ stopping site is antiparallel to the nearest Yb^{3+} moment. This nearest Yb neighbor also dominates the RKKY coupling field, which is parallel to the Yb^{3+} moment. Then the magnitude μ_{stat} of the static moment/Yb ion is approximately given by $\mu_{stat}\approx H_{stat}/|A^{RKKY}-A^{dip}|$, where A^{dip} is the dipolar coupling field constant at the μ^+ stopping site. This yields $\mu_{stat}\approx 2\times 10^{-3}\ \mu_B$, which is one of the smallest spontaneous moments found in a magnetically ordered compound.

It should be noted that the estimated value of the ordered Yb^{3+} moment does not change beyond a order of magnitude even if implanted muons stop at other possible sites, or if the magnetic structure is not that assumed above or is even disordered. The very small ordered Yb^{3+} moment seems consistent with the low $T_N\approx 70$ mK, and with the recent observation of a specific heat anomaly at T_N with a very small entropy release ($\sim 0.03R\ln 2$) (Ref. 38). Taken together, the data indicate that $YbRh_2Si_2$ is located quite close to the QCP.

C. Spin dynamics near a QCP

The exponentiality of the LF-μSR relaxation functions (Sec. II B) indicates that $YbRh_2Si_2$ is free from magnetic disorder and is in a single phase even far below the Kondo temperature. The Kondo disorder[29] and the Griffiths-phase[30]

mechanisms seem to be ruled out as the primary cause for the NFL behavior of this compound, although these two disorder-driven models have been considered as promising theories for explaining the NFL behavior in heavy-fermion alloys. Investigation of low-temperature muon spin dynamics is expected to yield additional information about the origin of the NFL behavior on $YbRh_2Si_2$. In the following we discuss the field and temperature dependence of the muon spin relaxation rate obtained from LF-μSR experiments.

As shown in Fig. 2, the relaxation function in small magnetic fields is a single exponential, as is the relaxation function observed in ^{29}Si NMR in the field range 1.5–25 kOe. These results suggest that the low-frequency spin dynamics are generally characterized by a single homogeneous fluctuation component.

The temporal correlation function $q(t)$ of the fluctuating muon local field $\delta\mathbf{B}_{\rm loc}(t)$ is defined by $q(t)=\langle \delta\mathbf{B}_{\rm loc}(t)\cdot\delta\mathbf{B}_{\rm loc}(0)\rangle/\langle|\delta B_{\rm loc}|^2\rangle$, where the angular brackets indicate a thermal average. If $q(t)$ is exponential, with correlation time τ_c, the field dependence of $1/T_1$ expected in LF-μSR measurements is

$$\frac{1}{T_1}=2\frac{\gamma_\mu^2\langle|\delta B_{\rm loc}|^2\rangle\tau_c}{1+\gamma_\mu^2H_L^2\tau_c^2}. \tag{17}$$

If, in addition, τ_c is independent of applied field, and $1/\tau_c \gtrsim \gamma_\mu\langle|\delta B_{\rm loc}|^2\rangle^{1/2}$, $1/T_1$ is expected to exhibit a H_L^{-2} dependence for $\gamma_\mu^2H_L^2\tau_c^2\gg 1$. This is inconsistent with the present experimental result $1/T_1\propto H_L^{-1}$ (Fig. 4). In addition, the estimated value of $B_{\rm loc}$ from TF-μSR experiments and the (small) value of $1/T_1$ yields $\tau_c\approx 10^{-10}$ s, so that the relaxation is in the motionally narrowed limit. Then $1/T_1 \approx 2\gamma_\mu^2\langle|\delta B_{\rm loc}|^2\rangle\tau_c(H,T)$. The field dependence of $1/T_1$ suggests that the correlation time itself has a field dependence for small longitudinal magnetic fields above $\sim$10 Oe.

The inverse field dependence of $1/T_1$ is consistent with the more general time-field scaling relation[27]

$$G(t,H)\propto G(t/H^\gamma) \tag{18}$$

with $\gamma\approx 1$, which is obeyed by the relaxation function data as shown in Fig. 8. Such time-field scaling can be derived for certain functional forms of $q(t)$ without assuming a specific form for the muon relaxation function. Following Keren *et al.*,[27] in the motionally narrowed limit the local muon polarization $G_{\rm loc}(t,H)$ relaxes exponentially with a rate $1/T_1 = 2\langle|B_{\rm loc}|^2\rangle\tau_c(H)$, where the correlation time $\tau_c(H)$ is given by

$$\tau_c(H)=\int_0^\infty q(t)\cos(\gamma_\mu Ht)dt. \tag{19}$$

Since T_N is hardly suppressed by magnetic fields $\lesssim$100 Oe, it is reasonable to consider that such small magnetic fields do not modify the spin-fluctuation spectrum. Thus the field dependence of $\tau_c(H)$ is ascribed to variation of the μ^+ Zeeman frequency $\omega_\mu=\gamma_\mu H$ rather than a direct effect of field on $q(t)$. When $q(t)$ exhibits stretched-law $[q(t)=ct^{-\alpha}]$ or power-exponential $(q(t)=c\exp[-(\lambda t)^\beta])$ behavior, a scaling law of the form of Eq. (18) is found,[27] with $\gamma=1-\alpha<1$ for power-law correlation and $\gamma=1+\beta>1$ for power-exponential correlation. Thus the present result $\gamma\approx 1$ implies that α or β is close to zero. This means that $q(t)$ is insensitive to t, suggesting that the spin-spin correlation time is quite long, and that the characteristic energy of spin fluctuations is quite small. Long correlation times (slow magnetic fluctuations) are generally expected in the critical region just above magnetic transitions.

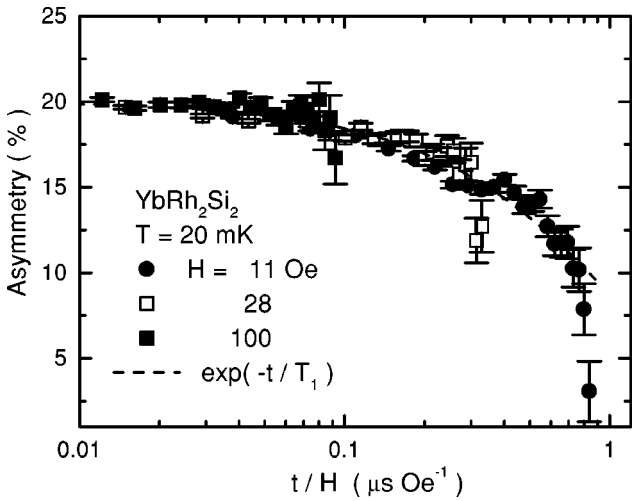

FIG. 8. μ^+ relaxation function data of the inset of Fig. 2 plotted versus the scaling variable t/H.

Figure 3 gives the temperature dependence of $1/T_1$ in a longitudinal field of 19 Oe. The absence of a clear anomaly near T_N is consistent with the observed small value of the static Yb^{3+} moment (Sec. III B), as expected in the vicinity of a QCP. If we assume that the entropy release at T_N is small and that quantum critical magnetic fluctuations survive below T_N, then the low-temperature muon relaxation should be dominated by these critical fluctuations. The long-lived correlations are therefore likely to be a characteristic feature of quantum critical fluctuations.

Over the temperature range 0.07–2 K the temperature dependence of $1/T_1$ (inset to Fig. 3) can be fit either to a logarithmic dependence $1/T_1\propto -\ln T$, or a power law $1/T_1 \propto T^{-0.17\pm 0.03}$. It is noteworthy that $1/T_1\approx -\ln T$ is the temperature dependence predicted by the self-consistent renormalization (SCR) theory[39] when the system is close to a two-dimensional (2D) AFM quantum critical point. If we take into consideration the fact that the characteristic NFL temperature dependences of the resistivity and specific heat $\Delta\rho\approx T$ and $\Delta C/T\approx -\ln T$ are also in agreement with temperature dependence near the 2D AFM critical point, the result $1/T_1\approx -\ln T$ seems to reinforce this scenario. However, recent specific-heat and magnetization measurements show that both quantities diverge as $H\rightarrow 500$ Oe and a very large Wilson ratio of about 14 (Ref. 18), which suggests the importance of ferromagnetic correlations. The experimental results reported so far seem to indicate that the behavior of spin fluctuations in $YbRh_2Si_2$ is complex, with appreciable peaks at wave vectors $\mathbf{q}=0$ and $\mathbf{q}=\mathbf{q}_0\neq 0$ in the dynamic

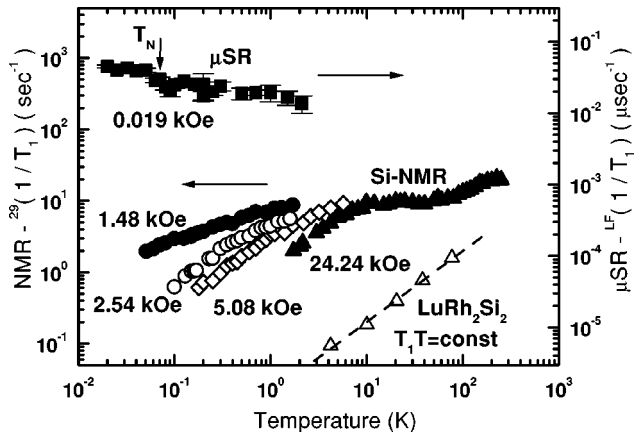

FIG. 9. Temperature and magnetic field dependence of $1/T_1$ in $YbRh_2Si_2$ as measured by ^{29}Si NMR [$^{29}(1/T_1)$] and μSR [$^{\mathrm{LF}}(1/T_1)$]. The left-hand and right-hand scales are for $^{29}(1/T_1)$ and $^{\mathrm{LF}}(1/T_1)$, respectively. The two scales are normalized to each other according to Eq. (20).

spin susceptibility. Complex magnetic fluctuations related to NFL behavior in $YbRh_2Si_2$ are also suggested by recent ^{29}Si NMR measurements.[16]

Quite recently, Si, Rabello, Ingersent, and Smith[40] have considered a new class of QCP in which localized moments with low-energy fluctuations can survive down to low T. In this scenario magnetic fluctuations at the QCP are long lived but exhibit local criticality if the interactions have a 2D character. According to this theory the spin-lattice relaxation rate $1/T_1$ is expected to be constant, consistent with the weak temperature dependence observed in the present experiment. The long-lived spin correlations at low temperatures revealed by the LF-μSR relaxation rates and the complex spin-fluctuation spectra near the QCP suggested by NMR experiments[16] are consistent with the magnetic character proposed by Si *et al.* Furthermore, $YbRh_2Si_2$ possesses the 2D crystal structure and anisotropic susceptibility required for applicability of this theory.

Finally, we compare the LF-μSR rate $^{\mathrm{LF}}(1/T_1)$ with the ^{29}Si NMR rate $^{29}(1/T_1)$ at low temperatures, measured in the field range 1.48–24.48 kOe.[16] It was found that $^{29}(1/T_1)$ also exhibits a remarkable dependence on applied fields, especially at low temperatures. From these results the field dependence is expected to be significant in magnetic fields less than 1.4 kOe, since the change in $^{29}(1/T_1)$ with applied field at low temperatures becomes larger at low fields (Fig. 9). The present μSR relaxation measurements probe spin fluctuations at the small field of 19 Oe, so that the μSR and NMR data are quite complementary. If we assume that both relaxation rates are determined by the same dynamical susceptibility $\chi''(q,\omega)$, then only the transferred hyperfine coupling constants are different between the two experiments. The ratio of the muon relaxation rate $^{\mathrm{LF}}(1/T_1)$ to the nuclear rate $^{29}(1/T_1)$ is then

$$\frac{^{\mathrm{LF}}(1/T_1)}{^{29}(1/T_1)} = \left(\frac{\gamma_\mu A_\mu}{\gamma_{\mathrm{Si}} A_{\mathrm{Si}}}\right)^2, \tag{20}$$

where γ_{Si} is the gyromagnetic ratio of the ^{29}Si nucleus and $A_{\mathrm{Si}} = -727$ G/μ_B is the hyperfine field at the Si site.[16] Figure 9 gives a comparison between $^{\mathrm{LF}}(1/T_1)$ and $^{29}(1/T_1)$, where the left-hand and right-hand scales are for $^{29}(1/T_1)$ and $^{\mathrm{LF}}(1/T_1)$ respectively, and the two scales are normalized to each other using Eq. (20). The normalized $^{\mathrm{LF}}(1/T_1)$ is approximately three orders of magnitude larger than the normalized $^{29}(1/T_1)$, which suggests that the spin dynamics have a very strong field dependence below 1.4 kOe. It is noteworthy that $^{\mathrm{LF}}(1/T_1)$ in 19 Oe, where the spin fluctuations are regarded to be the same as those in ZF, shows a small increase with decreasing temperature, whereas $^{29}(1/T_1)$ in magnetic fields greater than 1.45 kOe decreases with decreasing temperature. This result suggests that $1/T_1$ is dominated by QC fluctuations with a weak temperature dependence down to the lowest temperature, that these fluctuations are suppressed by applying external fields, and that a Fermi-liquid state is recovered at high fields (since the Korringa relation $1/T_1 \propto T$ is a characteristic feature of Fermi liquids). To understand the spin fluctuations at the QCP thoroughly, a neutron diffraction experiment that reveals the **q** dependence of the spin fluctuations would be very useful. In addition, the measurement of both $^{29}(1/T_1)$ and $^{\mathrm{LF}}(1/T_1)$ between 19 Oe and 1.4 kOe is needed to determine evolution of the spin-fluctuation character near QCP. These experiments are currently in progress.

IV. CONCLUSIONS

The μSR experiments described in this article yield information on the low-temperature behavior of the non-Fermi-liquid compound $YbRh_2Si_2$. The static Yb^{3+}-moment freezing inferred from other experiments at low temperatures[14] is confirmed, although the data do not determine the magnetic structure. The freezing temperature $T_N \approx 70$ mK is in good agreement with values found from resistivity and ac susceptibility measurements, and the magnetic order is found to be a bulk effect because it is experienced by the entire sample volume. The relaxation rate associated with the onset of the static magnetism yields a value of the static field $H_{\mathrm{stat}} \approx 2$ G at the μ^+ stopping site.

From TF-μSR experiments the relative spread $\delta K/|\overline{K}|$ of the μ^+ Knight shift remains constant over the temperature range 1.8–70 K; the lower temperature is a order of magnitude smaller than the Kondo temperature $T_K \approx 25$ K. This behavior is consistent with $\delta K/|\overline{K}|$ from the ^{29}Si NMR measurements, and indicates that any susceptibility inhomogeneity $\delta\chi$ originating from structural disorder is quite small in $YbRh_2Si_2$. Thus the compound $YbRh_2Si_2$ is ordered as well as stoichiometric, and disorder-driven NFL mechanisms are not expected to be applicable.

Candidate μ^+ stopping sites were considered from analyses of the TF-μSR Knight shift parameters, and the $4e[\frac{1}{2},\frac{1}{2},\frac{5}{16}]$ site was found to be the most probable site. Using the dipole fields and the transferred hyperfine field from Yb^{3+} spins at the site, the magnitude of the static Yb^{3+} moment below 70 mK is estimated as $\sim 2\times 10^{-3}\mu_B$ for a particular AFM ordered Yb^{3+}-moment structure. This small

value is not changed by orders of magnitude for different choices of the μ^+ stopping site, or for alternative ordered or disordered magnetic structures.

The muon spin-lattice relaxation function is exponential in longitudinal applied magnetic fields, again indicative of homogeneous behavior. The relaxation dynamic rate exhibits a power-law dependence $1/T_1 \propto H_L^{-1}$ on applied longitudinal field for $H_L \gtrsim 10$ Oe. This behavior is evidence for a long correlation time at the μ^+ stopping site, which is considered to be a characteristic feature of QC magnetic fluctuations. From the comparison of $1/T_1$ between μSR and NMR measurements the relaxation rate appears to increase anomalously in fields below 1 kOe. The relaxation below 1.4 kOe is considered to be intimately related to the critical fluctuation near the QCP. The present μSR studies reveal that $YbRh_2Si_2$ is a unique NFL compound, in which the NFL behavior is induced by homogeneous QC spin fluctuations.

ACKNOWLEDGMENTS

We are grateful to A. Amato, C. Baines, and D. Herlach, Paul Scherrer Institute, for help with these experiments. This

TABLE II. Calculated dipolar coupling field tensors $\mathbf{A}^{\mathrm{dip}}$ and approximate dipolar symmetry at candidate μ^+ stopping sites (multiplicity, Wyckoff letter, and relative bct axis coordinates) in $YbRh_2Si_2$. (The dipolar symmetry only appears after diagonalization.)

site	$\mathbf{A}^{\mathrm{dip}}$ (G/μ_B)	approx. dipolar symmetry
$2b[\frac{1}{2},\frac{1}{2},0]$	$\begin{pmatrix} 689 & 0 & 0 \\ 0 & 689 & 0 \\ 0 & 0 & -1378 \end{pmatrix}$	c-axis uniax.
$4c[\frac{1}{2},0,0]$	$\begin{pmatrix} 4393 & 0 & 0 \\ 0 & -2007 & 0 \\ 0 & 0 & -2386 \end{pmatrix}$	$\sim a$-axis uniax.
$4e[0,0,\frac{1}{4}]$	$\begin{pmatrix} -649 & 0 & 0 \\ 0 & -649 & 0 \\ 0 & 0 & 1298 \end{pmatrix}$	c-axis uniax.
$4e[\frac{1}{2},\frac{1}{2},\frac{5}{16}]$	$\begin{pmatrix} -1485 & 0 & 0 \\ 0 & -1485 & 0 \\ 0 & 0 & 2970 \end{pmatrix}$	c-axis uniax.
$8f[\frac{1}{4},\frac{1}{4},\frac{1}{4}]$	$\begin{pmatrix} -472 & 136 & 469 \\ 136 & -472 & 469 \\ 469 & 469 & 944 \end{pmatrix}$	$\sim$tilted uniax.
$8g[0,\frac{1}{2},\frac{1}{8}]$	$\begin{pmatrix} -1228 & 0 & 0 \\ 0 & 1403 & 0 \\ 0 & 0 & -175 \end{pmatrix}$	$\sim c$-axis extreme ortho.
$8g[\frac{1}{2},0,\frac{1}{16}]$	$\begin{pmatrix} 3273 & 0 & 0 \\ 0 & -1745 & 0 \\ 0 & 0 & -1528 \end{pmatrix}$	$\sim a$-axis uniax.
$8j[\frac{1}{2},\frac{1}{4},0]$	$\begin{pmatrix} 2150 & 0 & 0 \\ 0 & -325 & 0 \\ 0 & 0 & -1825 \end{pmatrix}$	$\sim a$-axis extreme ortho.
$16m[\frac{1}{4},\frac{1}{4},\frac{5}{32}]$	$\begin{pmatrix} -344 & 519 & 957 \\ 519 & -344 & 957 \\ 957 & 957 & 688 \end{pmatrix}$	$\sim$tilted uniax.
$16m[\frac{1}{8},\frac{1}{8},\frac{7}{32}]$	$\begin{pmatrix} -743 & 101 & 491 \\ 101 & -743 & 491 \\ 491 & 491 & 1486 \end{pmatrix}$	$\sim$tilted ortho.
$16n[\frac{1}{8},\frac{1}{2},\frac{3}{32}]$	$\begin{pmatrix} -1131 & 0 & 370 \\ 0 & 1923 & 0 \\ 370 & 0 & -792 \end{pmatrix}$	$\sim$tilted extreme ortho.

TABLE III. Dipolar and RKKY transferred hyperfine coupling fields (in units of G/μ_B) in $YbRh_2Si_2$, calculated from Eqs. (A5) and (A6) using the angular average $A_{av}^{hf}=-349$ G/μ_B and r.m.s. width $\delta A_{r.m.s.}^{hf}=399$ G/μ_B of the powder-pattern distribution from TF-μSR measurements (Sec. II C). The + and − signs refer to the sign of the discriminant in the solution of the quadratic Eq. (A6).

approx. dipolar symmetry	A_+^{dip}	A_-^{dip}	A_+^{RKKY}	A_-^{RKKY}
c-axis uniax.	2655	−5676	2112	−5610
~a-axis uniax.	333	−322	−503	−200
~c-axis extreme ortho.	492	−492	−349	−349
~a-axis extreme ortho.	485	−865	−574	52
~tilted uniax. $8f[\frac{1}{4},\frac{1}{4},\frac{1}{4}]$	1903	−2696	1011	−2275
~tilted uniax. $16m[\frac{1}{4},\frac{1}{4},\frac{5}{32}]$	656	−691	−112	−599
~tilted extreme ortho. $16n[\frac{1}{8},\frac{1}{2},\frac{3}{32}]$	503	−807	−542	−40

research was supported in part by the U.S. NSF, Grant Nos. DMR-9731361, DMR-0102293, and DMR-0203524, by the COE Research Grant No. (10CE2004) and 21 COE in Grant-in-Aid for Scientific Research from the Ministry of Education, Sport, Science, and Technology of Japan (MESST), and by the Grant-in-Aid for JPSJ and MESST.

APPENDIX: CANDIDATE MUON STOPPING SITES IN $YbRh_2Si_2$

This Appendix describes the calculation of transferred hyperfine coupling tensor elements from measured average shifts and r.m.s. widths of the powder-pattern-broadened TF-μSR spectra in $YbRh_2Si_2$. These ''experimental'' tensor elements can then be used to identify the most likely μ^+ stopping site. In particular, the dipolar coupling tensor can be compared with lattice-sum calculations. As in Sec. II B we assume that the RKKY coupling tensor $\mathbf{A}^{RKKY}$ is isotropic ($\mathbf{A}^{RKKY}=A^{RKKY}\mathbf{1}$). We also note that $\mathbf{A}^{dip}$ is a traceless tensor, so that two principal-axis elements suffice to specify it.

Candidate μ^+ stopping sites in the $YbRh_2Si_2$ tetragonal crystal structure are enumerated in Table II, along with the corresponding dipole coupling field tensors $\mathbf{A}^{dip}$ [Eq. (2)] evaluated in the body-centered tetragonal (bct) crystal reference frame. We consider only μ^+ stopping sites for which $\mathbf{A}^{dip}$ belongs (at least approximately) to one of the two following categories: uniaxial,

$$\mathbf{A}^{dip}=\begin{pmatrix} -A^{dip} & 0 & 0 \\ 0 & -A^{dip} & 0 \\ 0 & 0 & 2A^{dip} \end{pmatrix}, \tag{A1}$$

or ''extreme orthorhombic,''

$$\mathbf{A}^{dip}=\begin{pmatrix} -A^{dip} & 0 & 0 \\ 0 & A^{dip} & 0 \\ 0 & 0 & 0 \end{pmatrix} \tag{A2}$$

TABLE IV. Comparison of calculated and experimental values of dipolar coupling fields A^{dip} (in units of G/μ_B). A^{dip}(calc.): from Table II, Eq. (A1), and Eq. (A2). A^{dip}(exp): from Table III.

site	approx. dipolar symmetry	A^{dip} (calc)	A_+^{dip} (exp)	A_-^{dip} (exp)	OK?
$2b[\frac{1}{2},\frac{1}{2},0]$	c-axis uniax.	−689	2655	−5676	No
$4c[\frac{1}{2},0,0]$	~a-axis uniax.	2390	333	−322	No
$4e[0,0,\frac{1}{4}]$	c-axis uniax.	649	2655	−5676	No
$4e[\frac{1}{2},\frac{1}{2},\frac{5}{16}]$	c-axis uniax.	1485	2655	−5676	Yes [a]
$8f[\frac{1}{4},\frac{1}{4},\frac{1}{4}]$	~tilted uniax.	500	1903	−2696	No
$8g[0,\frac{1}{2},\frac{1}{8}]$	~c-axis extreme ortho.	−1300	492	−492	No
$8g[\frac{1}{2},0,\frac{1}{16}]$	~a-axis uniax.	1640	333	−322	No
$8j[\frac{1}{2},\frac{1}{4},0]$	~a-axis extreme ortho.	−1805	485	−865	No
$16m[\frac{1}{4},\frac{1}{4},\frac{5}{32}]$	~tilted uniax.	930	656	−691	? [a, b]
$16m[\frac{1}{8},\frac{1}{8},\frac{7}{32}]$	tilted ortho.	N/A [c]			
$16n[\frac{1}{8},\frac{1}{2},\frac{3}{32}]$	~tilted extreme ortho.	−1940	503	−807	No

[a] Rough match between A^{dip}(calc) and A_+^{dip}(exp).
[b] A^{RKKY}(exp)<0 (Table III).
[c] See Ref. 41.

(including permutations of the principal axes). Both of these classes are characterized by a single principal-axis element $A^{\rm dip}$ (Ref. 41).

These categories include all of the more symmetric sites, which are *a priori* the most likely μ^+ stopping sites. For these sites at least one principal axis of $\mathbf{A}^{\rm dip}$ is (at least approximately) in the basal (*ab*) plane. For most of these sites the *c* axis is also (at least approximately) a principal axis. Thus the dipolar coupling field tensor for these sites is (at least approximately) diagonal in the bct crystal reference frame. Approximate dipolar symmetries are summarized in Table II.

The bulk susceptibility tensor principal-axis elements are $\chi_\parallel$ and $\chi_\perp = r\chi_\parallel$ for field applied parallel and perpendicular to the *c* axis, respectively. Thus for the case where principal axes 1 and 2 of $\mathbf{A}^{\rm dip}$ are in the basal plane

$$K_{11}/\chi_\parallel = (A^{\rm RKKY} + A_{11}^{\rm dip})r,$$

$$K_{22}/\chi_\parallel = (A^{\rm RKKY} + A_{22}^{\rm dip})r,$$

$$K_{33}/\chi_\parallel = A^{\rm RKKY} - (A_{11}^{\rm dip} + A_{22}^{\rm dip}). \qquad \text{(A3)}$$

In addition, in an unaligned powder the average susceptibility $\chi_{\rm av}$ is given by

$$\chi_{\rm av} = \frac{1}{3}(2r+1)\chi_\parallel . \qquad \text{(A4)}$$

Equations (A3), (8), and (10) give $K_{\rm av}$ and $\delta K_{\rm r.m.s.}$ in terms of $A^{\rm RKKY}$ and the (diagonal) elements of $\mathbf{A}^{\rm dip}$. These can be reduced to one independent element $A^{\rm dip}$ using Eq. (A1) or Eq. (A2), whichever is applicable. Then the experimental values of $A_{\rm av}^{\rm hf} = N_A\mu_B K_{\rm av}/\chi_{\rm av}$ and $\delta A_{\rm r.m.s.}^{\rm hf} = N_A\mu_B \delta K_{\rm r.m.s.}/\chi_{\rm av}$ [Eqs. (13) and (14), respectively] allow us to write equations for the ''experimental'' values of $A^{\rm RKKY}$ and $A^{\rm dip}$ of the form

$$A_{\rm av}^{\rm hf} = A^{\rm RKKY} + tA^{\rm dip} \qquad \text{(A5)}$$

(the coefficient of $A^{\rm RKKY}$ is always 1) and

$$(\delta A_{\rm r.m.s.}^{\rm hf})^2 = u(A^{\rm RKKY})^2 + vA^{\rm RKKY}A^{\rm dip} + w(A^{\rm dip})^2, \qquad \text{(A6)}$$

where the coefficients *t*, *u*, *v*, and *w* are functions of the susceptibility anisotropy ratio r [~ 20 in $YbRh_2Si_2$ (Ref. 42)] that can be calculated for each of the dipole symmetries defined above. Equations (A5) and (A6) can then be solved for $A^{\rm RKKY}$ and $A^{\rm dip}$ in terms of $A_{\rm av}^{\rm hf}$ and $\delta A_{\rm r.m.s.}^{\rm hf}$. There are two sets of solutions because Eq. (A6) is quadratic.

For the $8f[\frac{1}{4},\frac{1}{4},\frac{1}{4}]$, $16m[\frac{1}{4},\frac{1}{4},\frac{5}{32}]$, $16m[\frac{1}{8},\frac{1}{8},\frac{7}{32}]$, and $16n[\frac{1}{8},\frac{1}{2},\frac{3}{32}]$ sites two principal axes are tilted (i.e., neither in the basal plane nor parallel to the *c* axis). Here the calculation is more complicated and involves the tilt angle θ. These ''tilted'' dipolar tensors then exhibit various approximate symmetries as summarized in Table II. All but the $16m[\frac{1}{8},\frac{1}{8},\frac{7}{32}]$ site[41] have either approximate uniaxial symmetry or approximate extreme orthorhombic symmetry in the principal-axis frame. The forms of Eqs. (A5) and (A6) are retained, with coefficients that depend on both r and θ. The resulting values of $A^{\rm RKKY}$ and $A^{\rm dip}$ are given in Table III.

To summarize the argument to this point: for a given dipolar symmetry these ''experimental'' values of $A^{\rm RKKY}$ and $A^{\rm dip}$ are the actual values if the μ^+ stopping site does in fact have that symmetry. Thus agreement (even rough agreement) between $A^{\rm dip}$(calc) calculated from a lattice sum [Eq. (2)] and an experimental value $A^{\rm dip}$(exp) (from Table III) is evidence for a possible μ^+ stopping site.

We note that $A^{\rm RKKY}$ is found to be positive in the majority of heavy-fermion systems studied to date.[19] Assuming this to be a general property, Table III allows us to rule out sites with $\sim a$-axis uniaxial or $\sim c$-axis extreme orthorhombic symmetry. The $16m[\frac{1}{4},\frac{1}{4},\frac{5}{32}]$ and $16n[\frac{1}{8},\frac{1}{2},\frac{3}{32}]$ sites are also ruled out by this criterion.

From the dipolar coupling field tensors of Table II (diagonalized where necessary) we determine the calculated values $A^{\rm dip}$(calc) as defined in Eq. (A1) or (A2), whichever is applicable. These are compared with experimental values $A^{\rm dip}$(exp) in Table IV, where it can be seen that only for the $4e[\frac{1}{2},\frac{1}{2},\frac{5}{16}]$ and $16m[\frac{1}{4},\frac{1}{4},\frac{5}{32}]$ sites is $A^{\rm dip}$(calc) in the neighborhood of one of the $A^{\rm dip}$(exp). The $16m[\frac{1}{4},\frac{1}{4},\frac{5}{32}]$ site is excluded if $A^{\rm RKKY}$ is taken to be positive, in which case the $4e[\frac{1}{2},\frac{1}{2},\frac{5}{16}]$ site is the most probable μ^+ stopping site.

*Present address: Department of Physics, Kyoto University, Kyoto 606-8502, Japan.

†Present address: Department of Physics, Faculty of Engineering, Tokushima University, Tokushima 770-8506, Japan.

[1] M.B. Maple, M.C. de Andrade, J. Herrmann, Y. Dalichaouch, D.A. Gajewski, C.L. Seaman, R. Chau, R. Movshovich, M.C. Aronson, and R. Osborn, J. Low Temp. Phys. **99**, 223 (1995); also *Proceedings of the Conference on Non-Fermi Liquid Behavior in Metals*, Santa Barbara, California, 1996, edited by P. Coleman, M.B. Maple, and A.J. Millis [J. Phys.: Condens. Matter **8**, 9675 (1996).]

[2] G.R. Stewart, Rev. Mod. Phys. **73**, 797 (2001).

[3] D. Jaccard, K. Behnia, and J. Sierro, Phys. Lett. A **163**, 475 (1992).

[4] N.D. Mathur, F.M. Grosche, S.R. Julian, I.R. Walker, D.M. Freye, R.K.W. Haselwimmer, and G.G. Lonzarich, Nature (London) **394**, 39 (1998).

[5] H. Hegger, C. Petrovic, E.G. Moshopoulou, M.F. Hundley, J.L. Sarrao, Z. Fisk, and J.D. Thompson, Phys. Rev. Lett. **84**, 4986 (2000).

[6] F. Steglich, J. Magn. Magn. Mater. **226-230**, 1 (2001).

[7] H.v. Löhneysen, T. Pietrus, G. Portisch, H.G. Schlager, A. Schröder, M. Sieck, and T. Trappmann, Phys. Rev. Lett. **72**, 3262 (1994).

[8] B. Andraka and G.R. Stewart, Phys. Rev. B **47**, 3208 (1993).

[9] F.M. Grosche, S.R. Julian, N.D. Mathur, F.V. Carter, and G.G. Lonzarich, Physica B **237-238**, 197 (1997).

[10] K. Ishida, Y. Kawasaki, T. Mito, C. Thessieu, G.-q. Zheng, Y. Kitaoka, C. Geibel, and F. Steglich, Hyperfine Interact. **128**, 193 (2000).

[11] Y. Kawasaki, K. Ishida, T. Mito, C. Thessieu, G.-q. Zheng, Y. Kitaoka, C. Geibel, and F. Steglich, Phys. Rev. B **63**, 140501(R) (2001).
[12] T. Mito, S. Kawasaki, G.-q. Zheng, Y. Kawasaki, K. Ishida, Y. Kitaoka, D. Aoki, Y. Haga, and Y. Onuki, Phys. Rev. B **63**, 220507(R) (2001).
[13] D.E. MacLaughlin, O.O. Bernal, R.H. Heffner, G.J. Nieuwenhuys, M.S. Rose, J.E. Sonier, B. Andraka, R. Chau, and M.B. Maple, Phys. Rev. Lett. **87**, 066402 (2001).
[14] O. Trovarelli, C. Geibel, S. Mederle, C. Langhammer, F.M. Grosche, P. Gegenwart, M. Lang, G. Sparn, and F. Steglich, Phys. Rev. Lett. **85**, 626 (2000).
[15] F. Steglich, N.K. Sato, N. Aso, P. Gegenwart, J. Custers, K. Neumaier, H. Wilhelm, C. Geibel, and O. Troverelli, Physica B **329-333**, 441 (2003).
[16] K. Ishida, K. Okamoto, Y. Kawasaki, Y. Kitaoka, O. Trovarelli, C. Geibel, and F. Steglich, Phys. Rev. Lett. **89**, 107202 (2002).
[17] C. Langhammer, doctoral dissertation.
[18] P. Gegenwart, J. Custers, C. Geibel, K. Neumaier, T. Tayama, K. Tenya, O. Trovarelli, and F. Steglich, Phys. Rev. Lett. **89**, 056402 (2002).
[19] A. Amato, Rev. Mod. Phys. **69**, 1119 (1997).
[20] NMR experiments at zero and low fields are possible using field-cycling techniques, but are technically difficult. See, for example, L.C. Hebel and C.P. Slichter, Phys. Rev. **113**, 1504 (1959); also A.G. Anderson and A.G. Redfield, *ibid.* **116**, 583 (1959).
[21] K. Ishida, D.E. MacLaughlin, O.O. Bernal, R.H. Heffner, G.J. Nieuwenhuys, O. Trovarelli, C. Geibel, and F. Steglich, Physica B **326**, 403 (2003).
[22] K. Ishida *et al.*, Physica B **329-333**, 589 (2003).
[23] A. Schenck, *Muon Spin Rotation Spectroscopy: Principles and Applications in Solid State Physics* (Hilger, Bristol, 1985).
[24] J.H. Brewer, in *Encyclopedia of Applied Physics*, edited by G.L. Trigg (VCH Publishers, New York, 1994), Vol. 11, p. 23.
[25] R. Kubo and T. Toyabe, in *Magnetic Resonance and Relaxation*, edited by R. Blinc (North-Holland, Amsterdam, 1967), p. 810.
[26] D.E. MacLaughlin *et al.*, Phys. Rev. B **37**, 3153 (1988).
[27] A. Keren, P. Mendels, I.A. Campbell, and J. Lord, Phys. Rev. Lett. **77**, 1386 (1996).
[28] O.O. Bernal, D.E. MacLaughlin, H.G. Lukefahr, and B. Andraka, Phys. Rev. Lett. **75**, 2023 (1995).
[29] E. Miranda, V. Dobrosavljević, and G. Kotliar, J. Phys.: Condens. Matter **8**, 9871 (1996); Phys. Rev. Lett. **78**, 290 (1997).
[30] A.H. Castro Neto, G. Castilla, and B.A. Jones, Phys. Rev. Lett. **81**, 3531 (1998).
[31] O.O. Bernal *et al.* Phys. Rev. B **54**, 13 000 (1996).
[32] C.-Y. Liu, D.E. MacLaughlin, A.H. Castro Neto, H.G. Lukefahr, J.D. Thompson, J.L. Sarrao, and Z. Fisk, Phys. Rev. B **61**, 432 (2000).
[33] D.E. MacLaughlin, O.O. Bernal, J.E. Sonier, R.H. Heffner, T. Taniguchi, and Y. Miyako, Phys. Rev. B **65**, 184401 (2002).
[34] C.H. Booth, D.E. MacLaughlin, R.H. Heffner, R. Chau, M.B. Maple, and G.H. Kwei, Phys. Rev. Lett. **81**, 3960 (1998).
[35] A. Amato, R. Feyerherm, F.N. Gygax, A. Schenck, J. Flouquet, and P. Lejay, Phys. Rev. B **50**, 619 (1994).
[36] Y. Yamamoto, S. Kawarazaki, Y. Miyako, K. Nishiyama, and K. Nagamine, Physica B **289-290**, 13 (2000).
[37] L.P. Le *et al.*, Phys. Rev. B **53**, R510 (1996).
[38] P. Gegenwart, J. Custers, T. Tayama, K. Tenya, C. Geibel, O. Trovarelli, F. Steglich, and K. Neumeier, Acta Phys. Pol. B **34**, 323 (2003).
[39] T. Moriya and T. Takimoto, J. Phys. Soc. Jpn. **64**, 960 (1995).
[40] Q. Si, S. Rabello, K. Ingersent, and J.L. Smith, Nature (London) **413**, 804 (2001).
[41] Sites that are neither uniaxial nor extreme orthorhombic have three independent coupling parameters (the two independent principal-axis elements of $\mathbf{A}^{\mathrm{dip}}$ and A^{RKKY}), which cannot be determined from only two experimental numbers (K and δK). Only the $16m[\frac{1}{8},\frac{1}{8},\frac{7}{32}]$ site is in this category, and it is not a likely candidate muon stopping site.
[42] O. Trovarelli, C. Geibel, C. Langhammer, S. Mederle, P. Gegenwart, F.M. Grosche, M. Lang, G. Sparn, and F. Steglich, Physica B **281&282**, 372 (2000).